Monthly Notices of the ROYAL ASTRONOMICAL SOCIETY

MNRAS **500,** 2012–2019 (2021) doi:10.1093/mnras/staa3497
Advance Access publication 2020 November 11

Kinematic complexity around NGC 419: resolving the proper motion of the cluster, the Small Magellanic Cloud, and the Magellanic bridge

Davide Massari [1,2]★ Silvia Raso,[1,3] Mattia Libralato [4] and Andrea Bellini[4]

[1]*INAF - Osservatorio di Astrofisica e Scienza dello Spazio di Bologna, Via Gobetti 93/3, I-40129 Bologna, Italy*
[2]*Kapteyn Astronomical Institute, University of Groningen, NL-9747 AD Groningen, The Netherlands*
[3]*Dipartimento di Fisica e Astronomia, Università degli Studi di Bologna, Via Gobetti 93/2, I-40129 Bologna, Italy*
[4]*Space Telescope Science Institute, 3700 San Martin Drive, Baltimore, MD 21218, USA*

Accepted 2020 November 6. Received 2020 November 5; in original form 2020 October 23

ABSTRACT

We present *Hubble Space Telescope* proper motions in the direction of the star cluster NGC 419 in the Small Magellanic Cloud. Because of the high precision of our measurements, for the first time it is possible to resolve the complex kinematics of the stellar populations located in the field, even along the tangential direction. In fact, the proper motions we measured allow us to separate cluster stars, which move on average with $(\mu_\alpha \cos\delta^{\rm NGC\,419}, \mu_\delta^{\rm NGC\,419}) = (+0.878 \pm 0.055, -1.246 \pm 0.048)$ mas yr^{-1}, from those of the Small Magellanic Cloud and those belonging to a third kinematic feature that we recognize as part of the Magellanic Bridge. Resolving such a kinematic complexity enables the construction of decontaminated colour–magnitude diagrams, as well as the measurement of the absolute proper motion of the three separate components. Our study therefore sets the first steps towards the possibility of dynamically investigating the Magellanic system by exploiting the resolved kinematics of its stellar clusters.

Key words: techniques: photometric – proper motions – galaxies: kinematics and dynamics – galaxies: individual: Magellanic Clouds.

1 INTRODUCTION

Star clusters are powerful tracers to investigate the formation and the evolutionary history of their host galaxies; in this respect, the study of their kinematics provides a wealth of information. The most immediate example is provided by the globular clusters (GCs) system of the Milky Way. Because of the recent combined availability of proper motion (PM) and spectroscopic radial velocity measurements, the orbits around the Milky Way for almost all of the known GC have been determined with great accuracy (Gaia Collaboration 2018; Baumgardt et al. 2019; Vasiliev 2019). By building up on these measurements, Massari, Koppelman & Helmi (2019) computed the GCs integrals of motion and were thus able to associate them to known (Ibata, Gilmore & Irwin 1994; Helmi et al. 2018; Koppelman et al. 2019; Myeong et al. 2019) and yet-to-be-discovered merger events that shaped the evolution of the Milky Way to its current structure (Kruijssen et al. 2020).

However, this kind of analysis is currently only feasible for the GC system of our Galaxy. The reason is that other extra-Galactic GC systems are too far away to be able to discern their proper motions from that of the hosting galaxy. In fact, the typical velocity difference between a GC and the stars of the surrounding environment is of the order of several tens of km s^{-1}, so that the required proper motion precision to resolve such a difference is of few tens of μas yr^{-1} and increases linearly with the distance. In the case of clusters embedded within the bulge of the hosting galaxy the situation is even worse, as the required velocity resolution drops to 5–10 km s^{-1}. Yet, even with the limited information provided by radial velocity alone, Mackey et al. (2019) were able to exploit the kinematics of the GC system of M31 to conclude that the galaxy likely experienced two significant merger events. Adding the full 3D kinematic information would therefore enable a much more detailed reconstruction of the evolutionary history of the galaxy.

One of the closest among other star cluster systems in the Local Group is that of the Magellanic Clouds (MCs). Despite being small satellites of the Milky Way (van der Marel et al. 2002; van der Marel & Kallivayalil 2014), according to ΛCDM cosmology they should still have experienced a complex history of merging events (e.g. Sales et al. 2013), and such a prediction has been recently supported by the dynamical confirmation that some of the ultrafaint dwarf galaxies orbiting the Milky Way are actually satellites of the Large Magellanic Cloud (LMC; Kallivayalil et al. 2018; Erkal & Belokurov 2020; Patel et al. 2020). Moreover, the existence of the Magellanic bridge connecting the LMC and the Small Magellanic Cloud (SMC) is a further evidence of interactions between the two (Zivick et al. 2019). Investigating the kinematics of the MCs star clusters system could therefore help reconstructing the MCs past history, yet resolving the clusters motion from that of the MC stellar populations has so far proved to be beyond the capabilities of current instrumentation like the *Gaia* mission.

One of the most effective ways to push the limits of astrometric measurements beyond the current boundaries is to increase, whenever possible, the temporal separation between different epochs of observations of the same object. In this respect, the *Hubble Space*

★ E-mail: davidemassari87@gmail.com

Table 1. List of *HST* images of NGC 419 used in this work.

Program ID	PI	Epoch (yyyy/mm)	Camera	Filter	Exposures N × t_{exp}
GO-10396	J. Gallagher	2006/01	ACS/WFC	F555W	1 × 20 s
				F814W	2 × 10 s
					4 × 474 s
		2006/07	ACS/WFC	F555W	2 × 20 s
					4 × 496 s
				F814W	2 × 10 s
					4 × 474 s
GO-12257	L. Girardi	2011/08	WFC3/UVIS	F336W	1 × 400 s
					1 × 690 s
					2 × 700 s
					1 × 740 s
GO-14069	N. Bastian	2016/08	WFC3/UVIS	F438W	1 × 70 s
					1 × 150 s
					1 × 350 s
					1 × 550 s
GO-15061	N. Bastian	2018/09	WFC3/UVIS	F336W	2 × 1395 s
					1 × 3036 s
				F438W	2 × 1454 s

Telescope (*HST*) is often superior to *Gaia*, as the latter is bound to scan the sky only for 5 yr during the nominal duration of the mission. This is why the most precise stellar proper motions have been measured either by *HST* (Bellini et al. 2018; Libralato et al. 2018, 2019) or by a combination of the two space-based telescopes (Massari et al. 2018, 2020). In this paper, we combine a set of long temporal baseline *HST* observations of the SMC cluster NGC 419 with the aim of resolving its motion from that of the surrounding stars. The success in achieving this objective could pave the road for the systematic investigation of the resolved 3D kinematics of the star clusters system of the MCs.

The paper is organized as follows. Section 2 presents the data set and the PM measurements. Section 3 describes the results we achieved on both NGC 419 and the SMC. The conclusions are provided in Section 4.

2 DATA ANALYSIS

We used the available *HST* images of NGC 419 from the Ultraviolet and Visible (UVIS) channel of the Wide Field Camera 3 (WFC3), obtained with the F336W and F438W filters, and from the Wide Field Channel (WFC) of the Advanced Camera for Surveys (ACS), obtained with the F555W and F814W filters. The list of the observations is given in Table 1, and the on-sky distrbution of each data set is shown in Fig. 1.

The photometric reduction was performed on the `_flc` images, which preserve the un-resampled pixel data for the stellar profile fitting and are corrected to remove charge transfer efficiency (see Anderson & Bedin 2010), following the prescription given in Bellini et al. (2017, 2018). We refer to the aforementioned papers for a detailed description of the photometric reduction procedure, which we only briefly summarize in the following. We first created a list of bright objects in the field through a one-pass, single finding procedure without neighbour subtraction, using spatially variable library point spread function (PSF) of the *HST* detectors,[1] which we fine-tuned to

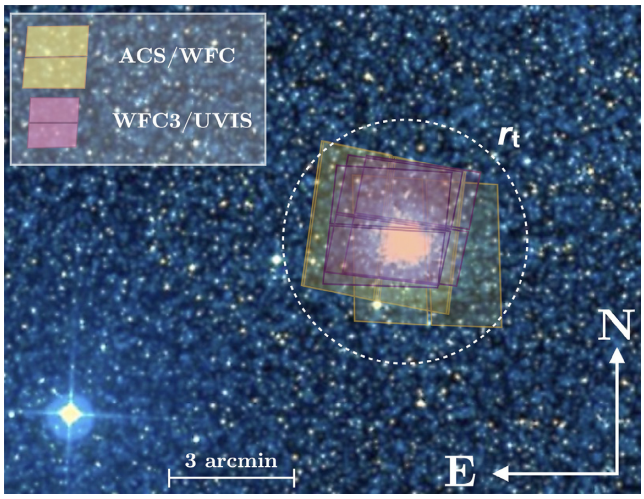

Figure 1. Sky distribution of the *HST* exposures used in the analysis. The yellow-shaded areas represent observations taken with ACS/WFC, the purple areas correspond to WFC3/UVIS data. The angular scale of the image, orientation, and tidal radius of the cluster ($r_t \simeq 174$ arcsec, Glatt et al. 2009) are marked in white. The stellar field in the background has been taken from `www.sky-map.org`.

each image using a set of bright, unsaturated, and relatively isolated stars. We corrected stellar positions for geometric distortion with the solutions reported in Anderson & King (2006), Bellini & Bedin (2009), and Bellini, Anderson & Bedin (2011). Secondly, we used the software `KS2` (see Bellini et al. 2017 for details) for a multipass photometry. This software is able to simultaneously perform the finding procedure on all the images and to subtract neighbouring sources. In this step, the stellar positions in each exposure are transformed, by means of six-parameter linear transformations, on to a common reference frame system, based on the stellar positions in the *Gaia* Data Release 2 (DR2) catalogue (Gaia Collaboration 2018). We calibrated the magnitudes to the `VEGAMAG` photometric system as described in Bellini et al. (2017) and Raso et al. (2019), by adding

[1] Publicly available at http://www.stsci.edu/~jayander/STDPSFs/.

to the instrumental magnitudes the photometric zero-point (ZP) of the considered filter, and the 3σ-clipped median difference between the aperture photometry[2] and the instrumental magnitudes.

The calibrated colour–magnitude diagram (CMD) of NGC 419 is shown in Fig. 2. The high photometric quality achieved allows us to recognize the complexity of the field in terms of stellar populations. The majority of the 44 739 measured stars is expected to belong to the stellar cluster NGC 419, of which it is easily possible to identify the extended main-sequence turn-off (eMSTO) and the sub-giant branch (SGB) regions. The surrounding SMC is clearly contaminating the CMD, as is evident from the young main sequence populating its bluest region. Yet, the way the SMC contaminates the cluster CMD is very difficult to describe precisely because of the intrinsic variety of its stellar populations. This is one of the aspects that our proper motion analysis will help to solve.

After the photometric reduction, a number of stars were rejected as poorly measured, based on several quality criteria. In particular, the sources that survived this photometric selection (about 34 000) were those for which (i) the quality of the PSF fit described by the QFIT[3] parameter (Bellini et al. 2017) is better than the 95th percentile of its distribution at any magnitude, (ii) the shape parameter RADSX (Bedin et al. 2008) is lower than the 95th percentile of its distribution at any magnitude, (iii) the fraction of light from neighbouring sources within the fitting radius is not larger than the light from the source itself.

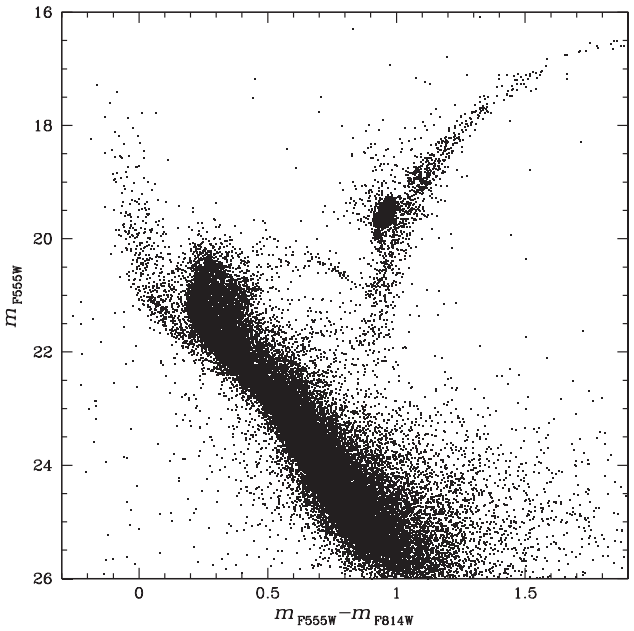

Figure 2. Optical m_{F555W} versus (m_{F555W}-m_{F814W}) CMD for all of the sources detected in the *HST* field surrounding the stellar cluster NGC 419.

2.1 Relative proper motions

Relative PMs were measured using the technique developed by Bellini et al. (2014) and improved in Bellini et al. (2018) and Libralato et al. (2018). A detailed description of the procedure, which we only briefly summarize here, can be found in those papers. The procedure to measure the relative PMs is iterative. Each iteration starts by cross-identifying stars in the raw catalogue of each exposure with those on the master frame, once their positions have been PM-shifted at the epoch of the raw catalogue. A six-parameter linear transformation determined using a set of reference bright and unsaturated cluster members is employed at this step. The use of cluster members is the reason why the PMs are measured relative to the bulk motion of the cluster, and thus have a zero mean value by definition. At the first iteration, stellar PMs are assumed to be zero, so that cluster members are defined based on their location on the CMD. For each star, the master-frame transformed positions as a function of epoch are fit with a least-squares straight line, the slope of which is a direct estimate of the star's PM. This fitting procedure is itself iterated after data rejection and sigma clipping. The last least-squares fit is performed with locally transformed master-frame stellar positions, based on the closest 45 reference stars, as this helps in correcting possible local geometric distortion residuals and thus in mitigating small-scale systematic effects. At the end of each iteration, the stellar cross-identification between the single exposures and master frames is improved by adjusting the master frame positions to match the epoch of each observation. The iterative process converges when the difference between master-frame positions from one iteration to the next are negligible. After convergence, we checked and corrected for spatially variable and colour-dependent systematic effects as described in Bellini et al. (2014).

Astrometric quality criteria were also applied in order to only select stars with reliable measurements. In particular, by following the prescriptions given in Libralato et al. (2019), we accepted stars for which (i) the reduced χ^2 of the PM fit is smaller than two in both PM components, (ii) the fraction of positional measurements effectively used for the PM fit is larger than 90 per cent, (iii) the error on the PM is smaller than the 95th percentile of the its distribution at any magnitude, and (iv) the error on the PM is smaller than 0.1 mas yr^{-1}. This leaved us with a total high-quality sample of about 19 000 stars. The behaviour of the PM uncertainty (see Bellini et al. 2018 for the details of its derivation) as a function of the m_{F555W} magnitude for this sample is shown in Fig. 3, where the best sources reach a PM precision of $\sim$10 μas yr^{-1}.

2.2 Absolute proper motions

HST relative astrometry has been historically brought to an absolute system using background galaxies and quasars since their absolute motions are known to be null due to their large distance. The main limitation of this method is the low number of this kind of faint objects in the typical *HST* field, combined with shallow exposures times and stellar crowdining. The typical precision achieved on the absolute PM ZPs using background anchors varies from $\sim$0.03 (Sohn et al. 2017) to 0.1–0.2 mas yr^{-1} (Massari et al. 2013, Libralato et al. 2019), depending on each individual case. This limitation can in principle be overcome using *Gaia* stars as a reference, as they are bright in *HST* images and significantly more numerous than suitable extragalactic calibrators, thus offering more accurate and precise registration to an absolute astrometric system (e.g. Libralato et al. 2020). For this reason, in this study we determined the absolute PM ZPs using the *Gaia* DR2 stars (Gaia Collaboration 2018) that are in common with our high-quality sample. The cross-match between the *Gaia* and our *HST* catalogues has been performed by means of the CATAPACK suit of

[2]The aperture photometry has been measured on the _drc images with a 8-pixel aperture, and corrected for the finite aperture, see https://stsci.edu/hst/instrumentation/wfc3/data-analysis/photometric-calibration.

[3]The QFIT value corresponds to the linear correlation coefficient between the pixel values and the PSF model.

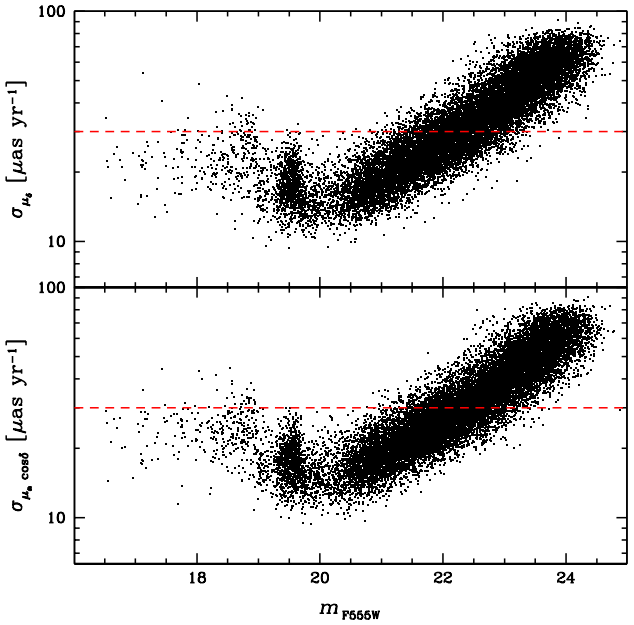

Figure 3. Distribution of PM errors as a function of the $m_{\rm F555W}$ magnitude for the sample of high-quality stars. The upper panel shows the PM error along declination, while the lower panel shows the PM error along right ascension. The red-dashed lines correspond to the cut-off criterion applied to select the high-quality sample.

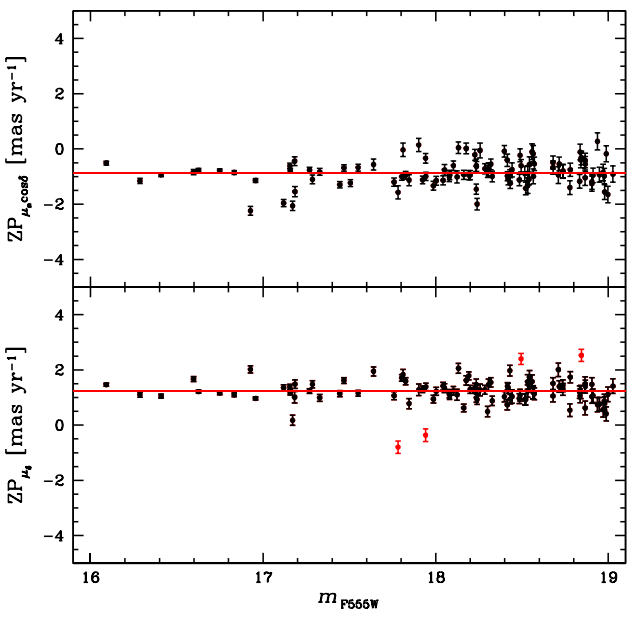

Figure 4. Absolute PM zero-points for the two components computed from the stars in common between our high-quality sample and the *Gaia* catalogue. The red symbols indicate stars excluded by the adopted iterative 3σ-clipping. The red solid lines mark the final mean zero-points.

software.[4] The adopted distance criterion for two stars to be matched is to have a separation smaller than 0.4 arcsec (which corresponds to the effective angular resolution of the *Gaia* DR2 observations, see Lindegren et al. 2018) and a difference in magnitude smaller than one mag. In this way, we select 1755 stars having both *HST* and *Gaia* proper motions. Before estimating the absolute ZP, though we apply some further quality cuts in order to have the best possible reference sample. In particular, we excluded all of the stars with renormalized unit weight error (ruwe) >1.4 (Lindegren et al. 2018), stars with *Gaia* proper motion uncertainty larger than 0.3 mas yr^{-1} and stars within a distance of 50 arcsec from the cluster centre, where crowding is more severe for *Gaia*. This leaves us with a total of 105 reference stars. The application of the 0.1 mas yr^{-1} PM error cut adopted for *HST* stars would have included only 24 stars, and this is why we chose a more generous cut for the *Gaia* stars. The difference between the selected *HST* and *Gaia* proper motions is shown in Fig. 4, where the error bars represent the associated 1σ uncertainties, and each PM component is plotted separately. In order to determine the absolute ZPs, we finally applied an iterative 3σ-clipping algorithm (rejected stars are shown in red in Fig. 4) that provided the following solution:

$$\mathrm{ZP}_{\mu_\alpha \cos\delta} = -0.878 \pm 0.055\,\mathrm{mas\,yr^{-1}},$$

$$\mathrm{ZP}_{\mu_\delta} = +1.226 \pm 0.048\,\mathrm{mas\,yr^{-1}},$$

where the quoted uncertainties are the sum in quadrature of two terms. The first term is given by the standard error of the mean value of the two distributions, while the second term describes the *Gaia* systematic error on its PMs, and amounts to 0.03 mas yr^{-1} (see Gaia Collaboration 2018). Neither of the two proper motion ZPs shows a trend with stellar magnitude, further supporting the quality of our selection.

Parallax effects on the measured astrometric shifts among the different epochs should also be quantified, as they are a source of systematic errors in our analysis. The mean *Gaia* parallax of the stars used to determine the ZPs is $\pi_{Gaia} = 0.07$ mas, while for the sources located in the SMC we can assume a typical parallax $\pi_{\rm SMC} = 0.017$ mas. By following the prescriptions given in Massari et al. (2013), such a difference in parallax translates to a maximum apparent PM of 0.008 mas yr^{-1}, which is negligible when compared to the uncertainty on the absolute PM ZPs.

The vector point diagram (VPD) resulting from the application of the ZPs is shown in Fig. 5. A further cut on the PM error, which we require to be smaller than 30 μas yr^{-1} in both components (see the red-dashed lines in Fig. 3), has been applied in order to highlight the most important kinematical features, and will be maintained throughout the rest of the analysis unless stated differently.

3 POPULATION SELECTIONS AND RESULTS

The aim of our analysis is to distinguish NGC 419 members from the surrounding SMC stars by exploiting their kinematics. In order to do so, we require two clean samples of stars belonging to the two different populations. We remark that we do not care about how complete these samples are at this stage, but rather that the contamination from other populations is as little as possible.

3.1 NGC 419

To select stars belonging to the star cluster, we adopted the following criteria:

(i) We only considered stars closer than 40 arcsec from NGC 419 centre, as the density of its members is obviously higher in the innermost regions.

[4] http://davide2.bo.astro.it/~paolo/Main/CataPack.html

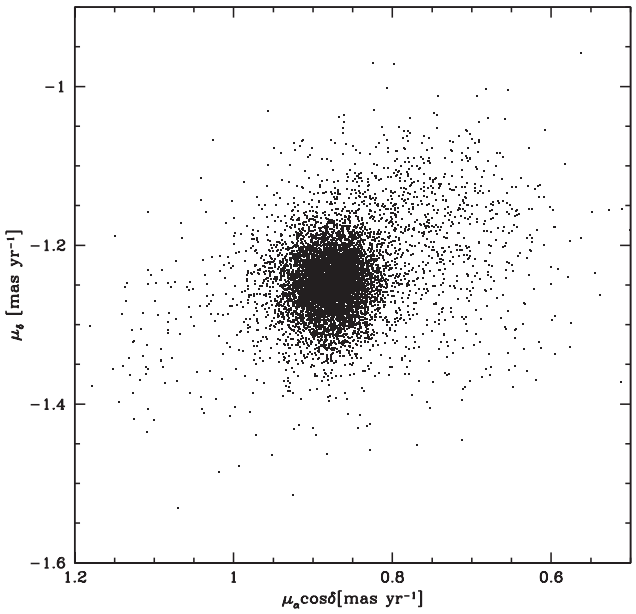

Figure 5. VPD for the stars belonging to the high-quality sample and with a PM error smaller than 30 μas yr^{-1} in both components.

(ii) We selected stars within 80 μas yr^{-1} from the mean motion of the bulk of sources in the VPD, which is at (0,0) mas yr^{-1} of the relative proper motion VPD, by construction.

The location on the CMD of this sample of NGC 419 stars is shown with the red dots in the left-hand panel of Fig. 6. NGC 419 is one of the first star clusters where an extended main-sequence turn-off has been detected (Glatt et al. 2008). Our selection leads to a CMD where this feature and the fainter main sequence are defined remarkably well, as well as the more evolved giant branches. Another peculiar photometric feature of NGC 419 is the so-called secondary red clump, which according to Girardi, Rubele & Kerber (2009) is due to the simultaneous presence in the cluster of stars that ignite Helium burning in degenerate and non-degenerate cores. These authors had already shown that the secondary red-clump is likely a genuine feature of the cluster, rather than made up of SMC stars, based on statistical arguments. Because of our proper motion analysis, here we can firmly confirm that the feature is in fact described by cluster members. We underline that, to our knowledge, this is the first kinematically decontaminated CMD of a GC in the MC ever presented in the literature. Even though the focus of this paper is the kinematics of the cluster and the SMC, our analysis shows that the proper-motion-based decontamination of CMDs of MC star clusters is now within the reach of *HST*.

Once a clean sample of cluster stars has been defined, it is possible to investigate its distribution in the VPD. This is shown in the right-hand panel of Fig. 6. The members of NGC 419 (the red symbols) clearly populate the bulk of the distribution. Since this is centred on the origin of the VPD of the relative proper motions by construction, the absolute proper motion of NGC 419 is given by the absolute proper motions ZPs, with opposite sign:

$$\mu_\alpha \cos\delta^{\rm NGC\,419} = +0.878 \pm 0.055\,{\rm mas\,yr^{-1}},$$

$$\mu_\delta^{\rm NGC\,419} = -1.226 \pm 0.048\,{\rm mas\,yr^{-1}}.$$

Coupled with the cluster position (Glatt et al. 2008), distance (∼59 kpc, Goudfrooij et al. 2014), and radial velocity of $v_{\rm sys}$ = 190.5 km s^{-1} (Kamann et al. 2018), our proper motion estimate enables future investigations of the dynamics of this system within the complex gravitational potential of the MCs.

3.2 SMC

A clean sample of SMC stars has to be selected among the sources that are not labelled as NGC 419 members. Given that the SMC stellar population is less numerous and has a larger velocity dispersion, a selection on the VPD is more subtle, as several SMC stars would end up within the limit of the cluster selection. For this reason, this time we preferred to exploit the CMD, and defined the following criteria:

(i) We selected stars more distant than 40 arcsec from NGC 419 centre.
(ii) We applied a colour cut such to select stars along the young main sequence, nominally $(m_{\rm F555W} - m_{\rm F814W}) < 0.1$.
(iii) We selected a region in the CMD that includes the faint and old SGB, at $0.6 < (m_{\rm F555W} - m_{\rm F814W}) < 1.1$ and $21 < m_{\rm F555W} < 22.2$.

The location of the SMC sample in shown in the left-hand panel of Fig. 6 as the blue points.

When looking at selected SMC stars in the VPD, two separate features stand out clearly. The first and more populated one is a broad clump of stars that trails NGC 419 along Right Ascension (RA), and is located at about $(\mu_\alpha \cos\delta, \mu_\delta) = (0.8, -1.15)$ mas yr^{-1}. The second feature is instead less populated and moves faster than the cluster along RA It is highlighted with the cyan symbols in the right-hand panel of Fig. 6 for sake of clarity.

In order to better interpret the nature of these two features, we first investigated their spatial distribution. As shown in Fig. 7, both are less centrally concentrated than the cluster, as expected for field populations. Moreover, their radial distribution is basically indistinguishable. A Kolmogorov–Smirnov test run on the two samples confirms that the probability for them to have been extracted from two populations sharing the same distribution on the sky is of 96.2 per cent.

On the other hand, a further inspection of the CMD revealed an important difference. As shown in Fig. 8, the stars belonging to the main feature (the blue points) populate both the young main sequence and the old SGB, regardless of the adopted combination of filters. Instead, the secondary feature is predominantly made up of young main-sequence stars (the cyan dots). We therefore recognize the main feature as the one describing the stellar component of the main body of the SMC. Its 3σ-clipped mean absolute proper motion amounts to

$$\mu_\alpha \cos\delta^{\rm SMC} = +0.777 \pm 0.005 \pm 0.055\,{\rm mas\,yr^{-1}}$$

$$\mu_\delta^{\rm SMC} = -1.141 \pm 0.003 \pm 0.048\,{\rm mas\,yr^{-1}},$$

where the second term of the associated uncertainty represents the error on the absolute proper motion ZPs. Our field lies about 1° off of the nominal centre of the SMC, which is moving away from us with a radial velocity of 145.6 km s^{-1} (Harris & Zaritsky 2006), at a distance of 63 kpc (Cioni et al. 2000). Prior to compare our measurements with others available in the literature, we must therefore correct for the perspective effect introduced by the different lines of sight. Using the formalism described in van de Ven et al. (2006) and Gaia Collaboration (2018), we obtain an estimate for the PM of the SMC centre of mass (COM) of

$$\mu_\alpha \cos\delta^{\rm SMC,COM} = +0.711 \pm 0.004 \pm 0.055\,{\rm mas\,yr^{-1}},$$

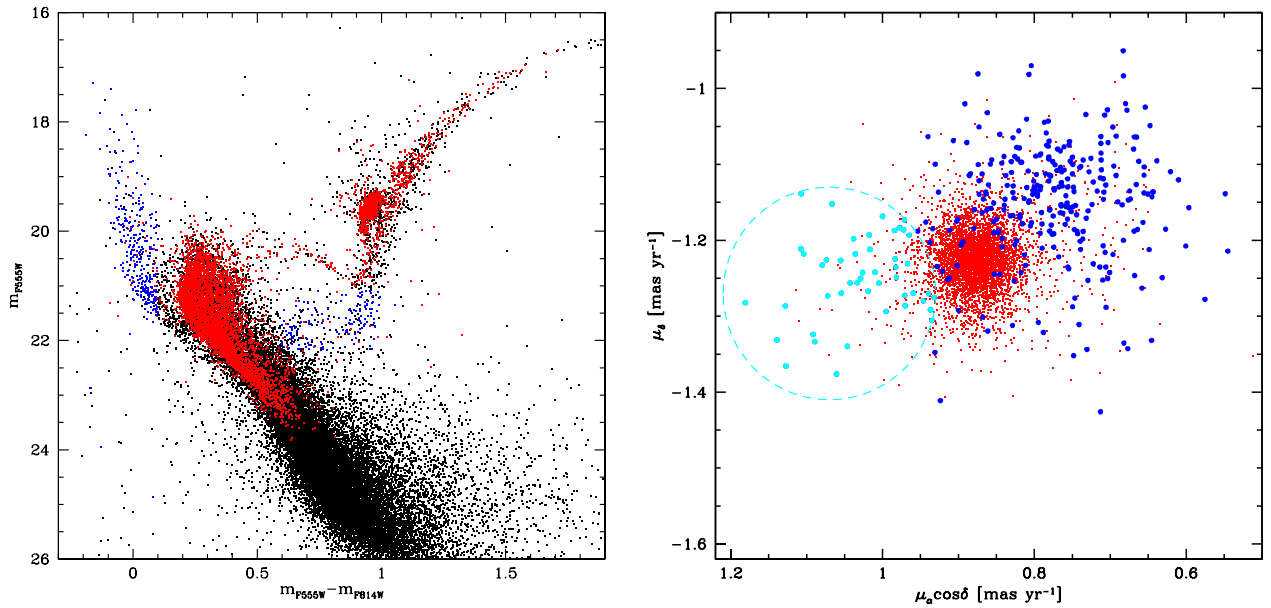

Figure 6. Left-hand panel: distribution in the CMD of the clean samples of cluster members (the red symbols) and SMC field stars (the blue symbols). Right-hand panel: distribution of the same samples in the VPD. SMC field stars split into two separated features, one trailing and one ahead of the GC. The latter is highlighted with the cyan symbols.

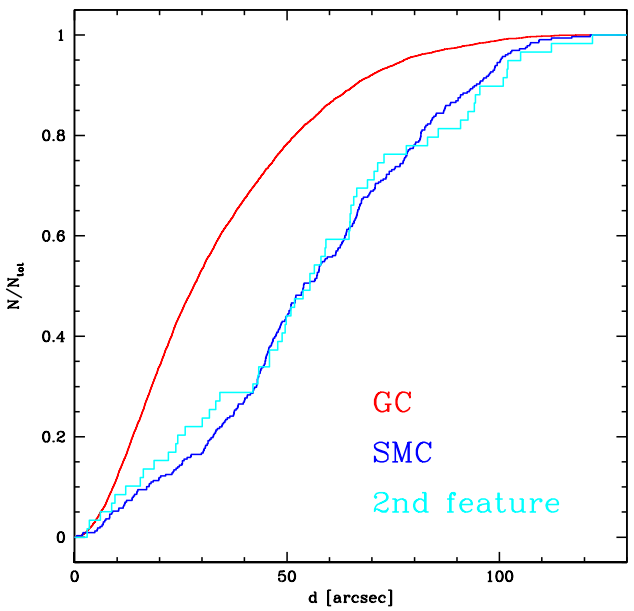

Figure 7. Radial distributions of cluster members (the red line), and the two sub-populations of SMC field stars (the blue and cyan symbols).

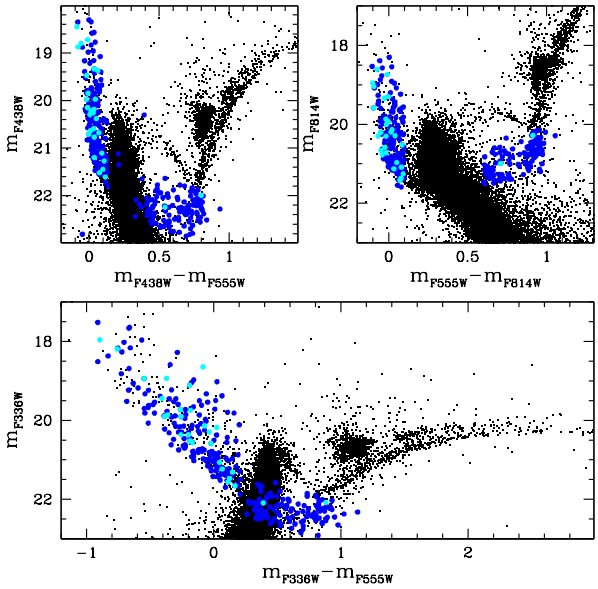

Figure 8. CMDs in different *HST* bands showing how the main SMC sub-population (the blue symbols) is made up of both young and old stars, while the secondary field sub-population (the cyan symbols) mainly includes young stars.

$\mu_\delta^{\rm SMC,COM} = -1.190 \pm 0.003 \pm 0.048$ mas yr^{-1}.

As a comparison, Kallivayalil et al. (2013) estimated the proper motion of the SMC COM to be $(\mu_\alpha \cos\delta,\ \mu_\delta) = (0.772 \pm 0.063,\ -1.117 \pm 0.061)$ mas yr^{-1}, whereas Gaia Collaboration (2018) estimated the mean PM of the SMC to be $(\mu_\alpha \cos\delta, \mu_\delta) = (0.797 \pm 0.030,\ -1.220 \pm 0.030)$ mas yr^{-1}. Both the results are in good agreement with our estimate.

The high quality of our PMs therefore allows us to clearly separate the motion of NGC 419 from that of the SMC. The net PM difference amounts to $\Delta\mu_\alpha \cos\delta = -0.1 \pm 0.005$ mas yr^{-1} along RA and to $\Delta\mu_\delta = 0.085 \pm 0.003$ mas yr^{-1} along declination, which at the distance of the SMC ($d_{\rm SMC} \sim 60$ kpc, Cioni et al. 2000; Muraveva et al. 2018) translates to an overall velocity difference of about 37.3 ± 1.4 km s^{-1}. This value exceeds the velocity dispersion that has been measured for the SMC from a sample of 2046 red giant stars by Harris & Zaritsky (2006), who found $v_{\rm disp} = 27.5 \pm 0.5$ km s^{-1}. We cannot draw any clear conclusion on whether or not such a difference is significant enough to advocate for a peculiar origin for

the cluster. However, given the young cluster age (∼1.5 Gyr, Glatt et al. 2008) and the lack of information on the anisotropy of SMC stars, we believe that our results reasonably support an in situ origin for NGC 419 within the SMC.

The secondary feature is thus made up of young stars, which are homogeneously distributed across the FoV as a field population. To verify whether these stars could belong to the Milky Way disc, we analysed their *Gaia* parallaxes and found out that they are too small (the median value is ∼0.02 mas) to be foreground contaminants (for which one should expect parallax values about one order of magnitude larger). The crucial piece of information to interpret this feature is ultimately given by the location of NGC 419 itself. Its coordinates lies at about 1° from the centre of the SMC and along the direction of the Magellanic bridge (Hindman, Kerr & McGee 1963). The Magellanic bridge is a gaseous structure connecting the two MCs that also hosts stars. The stellar component of the Bridge is mostly composed of young stars (Irwin, Kunkel & Demers 1985), though evidence for the presence of stars older than 1 Gyr also exists (e.g. Bagheri, Cioni & Napiwotzki 2013; Belokurov et al. 2017). The PM of stars in the Magellanic bridge has been very recently measured by Zivick et al. (2019) and Schmidt et al. (2020), and have lent further support to the hypothesis that this structure has formed from the past mutual interaction of the MCs (Besla et al. 2012). In Schmidt et al. (2020), in particular, the PM measurements extend from the LMC up to a distance of ∼4° from the SMC centre. The field around NGC 419 is even closer to the centre of the hosting galaxy, though, and this prevents a direct comparison with previous estimates. For the sample of stars belonging to the secondary feature of the VPD, we measure a mean absolute proper motion of

$$\mu_\alpha \cos\delta^{\rm Bridge} = +1.025 \pm 0.009 \pm 0.055\ {\rm mas\ yr^{-1}},$$

$$\mu_\delta^{\rm Bridge} = -1.247 \pm 0.007 \pm 0.048\ {\rm mas\ yr^{-1}}.$$

These values look consistent with the extrapolation towards smaller distances from the SMC centre of the N-body models presented by Schmidt et al. (2020), shown in their fig. 10. When transformed to an orthografic projection centred on the SMC using the equations given in Gaia Collaboration (2018), the PM of our secondary feature become $(\mu_x, \mu_y) = (0.210 \pm 0.055, -0.100 \pm 0.048)$ mas yr^{-1}. These values are also in reasonable agreement with the models described in Zivick et al. (2019).

Therefore, after putting together this kinematical information with the spatial and age-related arguments, we interpret the secondary feature of the VPD as made up of stars belonging to the Magellanic Bridge in the proximity of the SMC centre. Fig. 9 summarizes our findings by showing how NGC 419 (the red arrow) and the Bridge stars (the cyan arrow) move in a reference system centred on the SMC (marked with a green cross, the underlying density map is based on *Gaia* DR2 data and only includes sources brighter than $G = 19$) and where the SMC is at rest. If our interpretation is correct, then our measurements would provide a useful constraint on the overall kinematics of the Bridge in a region that has so far been unexplored.

4 SUMMARY AND CONCLUSIONS

We have analysed multiepochs *HST* observations of the SMC GC NGC 419 with the aim of measuring the PM of stars in its field. Our data set span a temporal baseline of 12.63 yr and, coupled with the exquisite astrometric capabilities of the telescope, allowed us to achieve proper motion measurements as precise as 10 μas yr^{-1}. With such a precision, we were able to resolve the intricate kinematics of the stellar populations sampled by our observations. In particular,

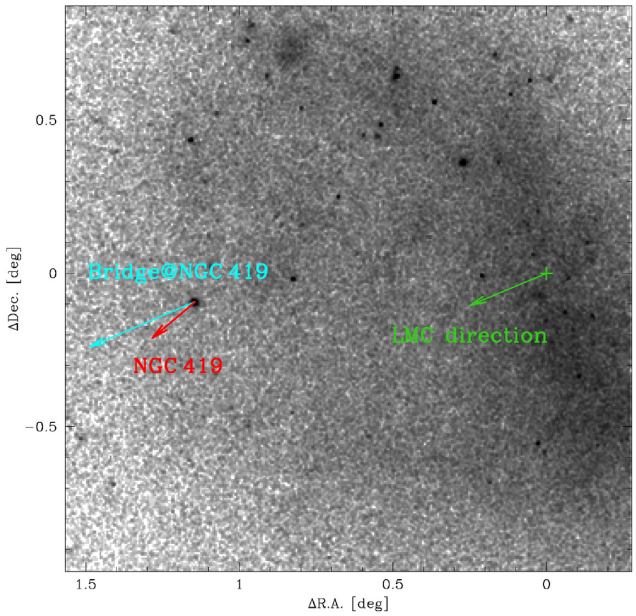

Figure 9. *Gaia* DR2 density map of the SMC showing the location of our field of view and the motion of NGC 419 and Magellanic Bridge stars in a reference system where the SMC is at rest. The direction connecting the SMC and the LMC centres is also shown as a green arrow.

(i) NGC 419 members were efficiently isolated from the field contaminants. The resulting CMD of the cluster confirmed the existence of peculiar features such as the eMSTO and the secondary red clump, which for the first time are decontaminated from non-member stars on an individual (and not statistical) basis;

(ii) the presence of stars with a *Gaia* DR2 PM measurements in our field allowed us to determine the absolute PM of NGC 419, which is $\mu_\alpha \cos\delta^{\rm NGC\,419} = +0.878 \pm 0.055$ mas yr^{-1}, $\mu_\delta^{\rm NGC\,419} = -1.226 \pm 0.048$ mas yr^{-1};

(iii) field stars clearly describe a main, homogeneous feature in the VPD, populated by both young and old stars. We associated this feature to stellar component of the main body of the SMC, and determine its perspective corrected absolute proper motion to be $\mu_\alpha \cos\delta^{\rm SMC,\,COM} = +0.711 \pm 0.004 \pm 0.055$ mas yr^{-1}, $\mu_\delta^{\rm SMC,COM} = -1.190 \pm 0.003 \pm 0.048$ mas yr^{-1}, in excellent agreement with previous measurements;

(iv) a few field stars clump around a secondary feature of the VPD that is solely populated by young stars, and which bulk motion is $\mu_\alpha \cos\delta^{\rm Bridge} = +1.025 \pm 0.009 \pm 0.055$ mas yr^{-1}, $\mu_\delta^{\rm Bridge} = -1.247 \pm 0.007 \pm 0.048$ mas yr^{-1}. Based on the location of these stars on the sky and on their measured kinematics, we interpret them as belonging to the Magellanic Bridge. Our PMs seem to confirm N-body predictions for such a feature presented by Schmidt et al. (2020), when extrapolated to the position of our field.

Recently, Omkumar et al. (2020) reported on the detection of a kinematically distinct sub-structure in front of the SMC, which is particularly dominant between 2.5° and 5° from the SMC centre. This sub-structure has a PM very similar to the one we measured for our secondary feature, and was interpreted by the authors as the result of tidal stripping from the Magellanic Bridge. Given that the kinematic properties of their sub-structure and our secondary component are fairly consistent, the two features might belong to the same population of Magellanic Bridge stars, which we sampled at a closer distance to the centre of the host galaxy. Future spectroscopic,

radial velocity measurements could help in confirming the possible common origin of these two populations.

Because of their large distance and high density, it is challenging to study the star clusters of the MCs, even for instruments such as those onboard the *Gaia* mission. In this paper, we demonstrate that the availability of multiepoch *HST* observations makes it possible to resolve and investigate the kinematics of the stellar population in the fields of MC clusters. On one hand, this will enhance the photometric investigation of elusive features in the CMD of MC star clusters, which can be strongly contaminated by field sources. On the other hand, resolving the clusters' 3D kinematics around the host galaxies will enable dynamical investigations that can shed light on the assembly histories of the MCs (e.g. Piatti, Alfaro & Cantat-Gaudin 2019), in turn providing important constraints on the shape of the MCs' gravitational potentials.

ACKNOWLEDGEMENTS

We warmly thank the anonymous referee for the constructive report that improved the quality of the paper. Based on observations made with the NASA/ESA *HST*, obtained from the data archive at the Space Telescope Science Institute. STScI is operated by the Association of Universities for Research in Astronomy, Inc. under NASA contract NAS 5-26555. This work has used data from the European Space Agency (ESA) mission *Gaia* (http://www.cosmos.esa.int/gaia), processed by the *Gaia* Data Processing and Analysis Consortium (DPAC, `http://www.cosmos.esa.int/web/gaia/dpac/consortium`). Funding for the DPAC has been provided by national institutions, in particular the institutions participating in the *Gaia* Multilateral Agreement.

DATA AVAILABILITY STATEMENT

The data underlying this article will be shared on reasonable request to the corresponding author.

REFERENCES

Anderson J., Bedin L. R., 2010, PASP, 122, 1035
Anderson J., King I. R., 2006, Instrument Science Report ACS 2006-01, Available at: http://www.stsci.edu/hst/acs/documents/isrs/isr0601.pdf
Bagheri G., Cioni M.-R. L., Napiwotzki R., 2013, A&A, 551, A78
Baumgardt H., Hilker M., Sollima A., Bellini A., 2019, MNRAS, 482, 5138
Bedin L. R., King I. R., Anderson J., Piotto G., Salaris M., Cassisi S., Serenelli A., 2008, ApJ, 678, 1279
Bellini A. et al., 2018, ApJ, 853, 86
Bellini A., Bedin L. R., 2009, PASP, 121, 1419
Bellini A., Anderson J., Bedin L. R., 2011, PASP, 123, 622
Bellini A. et al., 2014, ApJ, 797, 115
Bellini A., Bianchini P., Varri A. L., Anderson J., Piotto G., van der Marel R. P., Vesperini E., Watkins L. L., 2017, ApJ, 844, 167
Belokurov V., Erkal D., Deason A. J., Koposov S. E., De Angeli F., Evans D. W., Fraternali F., Mackey D., 2017, MNRAS, 466, 4711
Besla G., Kallivayalil N., Hernquist L., van der Marel R. P., Cox T. J., Kereš D., 2012, MNRAS, 421, 2109
Cioni M.-R. L., van der Marel R. P., Loup C., Habing H. J., 2000, A&A, 359, 601
Erkal D., Belokurov V. A., 2020, MNRAS, 495, 2554
Gaia Collaboration, 2018, A&A, 616, A12
Gaia Collaboration, 2018, A&A, 616, A1
Girardi L., Rubele S., Kerber L., 2009, MNRAS, 394, L74
Glatt K. et al., 2008, AJ, 136, 1703
Glatt K. et al., 2009, AJ, 138, 1403
Goudfrooij P. et al., 2014, ApJ, 797, 35
Harris J., Zaritsky D., 2006, AJ, 131, 2514
Helmi A., Babusiaux C., Koppelman H. H., Massari D., Veljanoski J., Brown A. G. A., 2018, Nature, 563, 85
Hindman J. V., Kerr F. J., McGee R. X., 1963, Aust. J. Phys., 16, 570
Ibata R. A., Gilmore G., Irwin M. J., 1994, Nature, 370, 194
Irwin M. J., Kunkel W. E., Demers S., 1985, Nature, 318, 160
Kallivayalil N., van der Marel R. P., Besla G., Anderson J., Alcock C., 2013, ApJ, 764, 161
Kallivayalil N. et al., 2018, ApJ, 867, 19
Kamann S. et al., 2018, MNRAS, 480, 1689
Koppelman H. H., Helmi A., Massari D., Roelenga S., Bastian U., 2019, A&A, 625, A5
Kruijssen J. M. D. et al., 2020, MNRAS, 498, 2472
Libralato M. et al., 2018, ApJ, 861, 99
Libralato M. et al., 2019, ApJ, 873, 109
Libralato M., Fardal M., Lennon D., van der Marel R. P., Bellini A., 2020, MNRAS, 497, 4733
Lindegren L. et al., 2018, A&A, 616, A2
Mackey D. et al., 2019, Nature, 574, 69
Massari D., Bellini A., Ferraro F. R., van der Marel R. P., Anderson J., Dalessandro E., Lanzoni B., 2013, ApJ, 779, 81
Massari D., Breddels M. A., Helmi A., Posti L., Brown A. G. A., Tolstoy E., 2018, Nat. Astron., 2, 156
Massari D., Koppelman H. H., Helmi A., 2019, A&A, 630, L4
Massari D., Helmi A., Mucciarelli A., Sales L. V., Spina L., Tolstoy E., 2020, A&A, 633, A36
Muraveva T. et al., 2018, MNRAS, 473, 3131
Myeong G. C., Vasiliev E., Iorio G., Evans N. W., Belokurov V., 2019, MNRAS, 488, 1235
Omkumar A. O. et al., 2020, MNRAS, tmp.3030O
Patel E. et al., 2020, ApJ, 893, 121
Piatti A. E., Alfaro E. J., Cantat-Gaudin T., 2019, MNRAS, 484, L19
Raso S. et al., 2019, ApJ, 879, 56
Sales L. V., Wang W., White S. D. M., Navarro J. F., 2013, MNRAS, 428, 573
Schmidt T. et al., 2020, A&A, 641, A134
Sohn S. T. et al., 2017, ApJ, 849, 93
van de Ven G., van den Bosch R. C. E., Verolme E. K., de Zeeuw P. T., 2006, A&A, 445, 513
van der Marel R. P., Kallivayalil N., 2014, ApJ, 781, 121
van der Marel R. P., Alves D. R., Hardy E., Suntzeff N. B., 2002, AJ, 124, 2639
Vasiliev E., 2019, MNRAS, 484, 2832
Zivick P. et al., 2019, ApJ, 874, 78

This paper has been typeset from a TEX/LATEX file prepared by the author.